Removal of Maxilon Red Dye by Adsorption and Photocatalysis: Optimum Conditions, Equilibrium, and Kinetic Studies

Mekatel, Elhadj*[+]***; Dahdouh, Nadjib; Amokrane, Samira; Nibou, Djamel***

Laboratory of Materials Technology, Faculty of Mechanic and Engineering Process (USTHB), B.P. 32, El-Alia, Bab-Ezzouar, Algiers, ALGERIA

Trari, Mohamed

Laboratory of Storage and Valorization of Renewable Energies, Faculty of Chemistry (USTHB), B.P. 32, Algiers, ALGERIA

ABSTRACT: *The present work has for the main objective the elimination of the textile dye Maxilon Red (MR) by coupling two processes, adsorption on activated clay followed by photocatalysis over the wurtzite ZnO. The influence of the physical parameters like the initial pH, adsorbent dose of the activated clay, MR concentration, and temperature have been studied. The best adsorption yield occurs at neutral pH ~ 7 within 60 min with an adsorption percentage of 97% for MR concentration of 25 mg/L and an adsorbent dose of 0.5 g/L. The data were suitably fitted by the Langmuir model with a maximum adsorption capacity of 175 mg/g. To investigate the adsorption mechanism, the adsorption constants were determined from the pseudo-first-order, pseudo-second-order, and intraparticle diffusion models. It was found that the MR adsorption is well described by the pseudo-second-order kinetic. The thermodynamic parameters* ΔH° *= -17.138 kJ/mol,* ΔS° *= 32.84 J/mol.K, and* $\Delta G^\circ = -6.419$ *to* -7.329 *kJ/mol with rising temperature from 25 to 50°C indicated that the adsorption is exothermic and spontaneous. The second part of this work was devoted to the photocatalytic degradation onto ZnO under solar irradiation of the residual MR concentration, which remained after adsorption. In this respect, the effect of ZnO dose and MR concentration has also been investigated. The photodegradation rate reached 99% under irradiation within 90 minutes under the optimum conditions. The parametric study showed that the elimination is very effective by photocatalysis, based essentially on the in situ generations of free radicals* $^{\bullet}OH$ *which are non-selective and very reactive. The present study shows that the activated clay is an effective low-cost adsorbent for the removal of Maxilon red from an aqueous solution.*

KEYWORDS: *Maxilon Red; Activated clay; Adsorption; Photodegradation; ZnO.*

INTRODUCTION

The industry of textile dyeing is one of the major responsible to environmental pollution because of the massive discharge of wastewater containing a multitude of dyes at high concentrations [1-3]. The presence of these colorants in water is not only aesthetically displeasing but are hazardous to biological organisms, human bodies and ecologies [4-6]. Maxilon Red GRL is an industrial azo dye, used as a model compound, and represents more than a half

***** *To whom correspondence should be addressed.*
+ E-mail: hmekatel@yahoo.fr
1021-9986/2021/1/93-110 18/$/6.08

of the global dye production [7]. Maxilon Red has been identified as one of the most problematic dyes, present in the industrial effluents, which can be potentially life threatening for living organisms [8-10]. Various physicochemical and biological treatment techniques have been documented to eliminate dyes at least below the threshold imposed by the World Health Organization [11-13]. The adsorption is widely employed in the water purification; the principle is to trap pollutants by an effective adsorbent through physical and/or chemical interactions [14-16]. Several materials are mainly derived from sources like zeolites [17], activated carbons [18], multiwall carbon nanotubes [19], chitosan [20], supported semiconductors [21] and clays [22, 23]. In this regard, the adsorption on clay is a practical and low cost way. However, clay must be treated with acid, organic molecules, treatments with cationic surfactants and polymer addition to improve to their performances [24-25]. On the other hand, advanced oxidation processes (AOPs) are attractive and complementary method for the treatment of textile wastewater effluents [26]. AOPs use strong oxidizing substances, such as hydrogen peroxide [27], ozone [28] and Fenton's reagent [29], to partially or completely degrade the organic matter (dyes, pesticides, drugs etc…). To improve the efficiency of conventional oxidation techniques AOPs using multiple oxidation technologies simultaneously have been developed, including photo-Fenton process [30], UV photolysis [31], sonolysis [32] and heterogeneous photocatalysis [33-35]. The latter is a clean alternative in the environmental engineering, currently extended to pilot scales for industrial goals. Its main advantages are low cost, low energy consumption with a variety of organic pollutants to treat and high mineralization degree. nevertheless, its application remains still limited to low pollutants concentrations and can be used as downstream. Indeed, high dyes concentrations stop considerably the penetration of the light which does not reach the catalyst powder and inhibit considerably AOPs. The combined adsorption/heterogeneous photocatalysis appear an efficient and elegant method which brings together the advantages of both processes [36-39]. In this respect, acid activated clay find industrial applications as bleaching earth, catalysts and catalyst supports and acid attack is a useful to modify the clay. In this study, we were interested by the treatment of waters containing an azo dye namely the Maxilon Red (MR) through adsorption by activated clay (AC) followed by photocatalysis on ZnO under sunlight. The remaining MR concentration after adsorption was removed by photocatalysis through $^{\bullet}OH$ radicals.

EXPERIMENTAL SECTION

Materials

All chemicals used in the experimental study were of analytical grade quality. The Maxilon red MR (> 98% purity, Fig. 1) was provided from Aldrich. HCl (37%), H_2SO_4 (98%) and NaOH (> 99% purity) were purchased from Merck company. Distilled water (0.9 MΩ cm) was used for preparing the solutions.

Analysis methods

The morphology of the powder of the raw clay and activated clay was examined by scanning electronic microscopy (SEM Philips XL 30, used voltage 10 KV). The X-ray diffraction (XRD) was performed with a Phillips PW 1800 diffractometer using Cu Kα radiation (λ= 0.154178 nm); the data were collected over the 2θ range (10 - 70°) at a scan rate of 0.5° min $^{-1}$. FT-IR analyses were performed within the range (450 - 4000 cm^{-1}) with a BRUKER Spectrum equipment (Germany). The MR concentrations were determined with a UV-Vis spectrophotometer Optizen 2120 UV-Visible (λ_{max} = 530 nm).

Preparation of the adsorbent

The clay used in this work was a Bentonite from Laghouat (~ 600 km South Algeria). It was thoroughly washed by dispersion in water. In order to activate the clay, 10 g was mixed with 100 mL of HCl (1 M) at 100 °C during 6 h, the content was separated from the solution and washed several times until complete Cl^- removal (negative test with $AgNO_3$) and dried at 100 °C overnight.

Adsorption and photocatalysis experiments

Batch adsorption experiments of MR were carried in a double walled Pyrex reactor of 250 cm^3 capacity whose temperature was regulated with a thermostatic bath. The MR solutions (25 - 125 mg/L) were prepared by dilution from a stock solution (1000 mg/L, Merck, 99.5%). The effect of pH on the adsorption was examined over the pH range (3 - 9), it was adjusted with NaOH (0.1 N) or H_2SO_4 (0.1 N) and measured with a Hanna HI 2210 pH-meter. The kinetics, isotherms at various MR concentrations

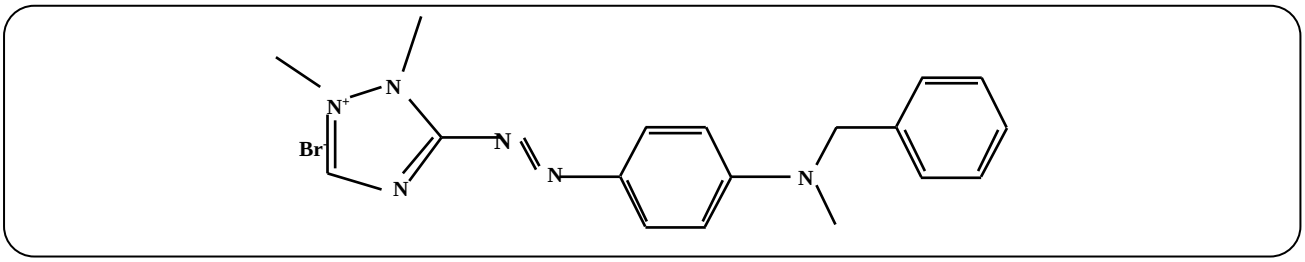

Fig. 1: Chemical structure of Maxilon Red.

(25 - 125 mg/L) and equilibrium adsorption were performed in the temperature range (25 – 50 °C). The removal efficiency (%) and the adsorption capacity q_e and q_t (mg/g) are given from the relation:

$$MR\ removal(\%) = \frac{(C_{in} - C_{fin})}{C_{in}} \times 100 \quad (1)$$

$$q_e = \frac{(C_{in} - C_{fin})V}{M} \quad (2)$$

$$q_t = \frac{(C_{in} - C_t)\ V}{M} \quad (3)$$

where C_{in} , C_{fin} and C_t are the initial and final MR concentration (mg/L), V is the volume of the solution (L) and M is the adsorbent dose (g). The remaining MR concentration after adsorption was treated by heterogeneous photocatalysis on ZnO exposed to solar light. ZnO was synthesized from zinc acetate (Zn $(CH_3COO)_2$, Sigma-Aldrich, > 98% purity) at 350 °C in a ventilated place.

The photodegradation was realized in a double walled borosilicate reactor connected to a thermo stated bath whose temperature was regulated at 25 °C. The powder was magnetically dispersed (300 rpm) and reactor was exposed to solar light (July); the incident flux (980 mW cm^{-2}) was measured with a calibrated light meter (Testo 545). The photodegradation efficiency of MR was calculated from the following relation:

$$MR\ photodegradation(\%) = \frac{(C_r - C)}{C_r} \times 100 \quad (4)$$

Where C_r is the the remaining *MR* concentration, and *C* is the maxilon red dye residual concentration in solution.

RESULTS AND DISCUSSION

Characterization

The powder XRD pattern of the raw clay (Fig. 2 a) shows the presence of the mineral clay including the main crystalline clay phases like (Illite at 9.97 Å (8.88°, 20%), Clinochlore at 7.14 Å (12.2°, 5%), Orhtoclase at 3.77 Å (23.5°, 5%) and Albite at 6.41 and 3.18 Å (14° and 28°) and non-clay phases as Quartz at 4.26 Å (20.9°, 70%), 3.34 Å (26.6°) and 2.45 Å (36.6°) and Calcite at 3.03 Å (29.5°, 5%). The indexation of XRD peaks was realized according to the JCPDS Cards [40]. The XRD pattern of the crude clay after chemical treatment by HCl solution (Fig. 2 b) has remained nearly intact and therefore the chemical treatment did not influence its structure as shown by XRD analysis.

The XRD pattern of ZnO (Fig. 2 c) is in perfect agreement with the hexagonal wurtzite ZnO structure (JCPDS 01-080-0075).

Fig. 2 shows texture of the clay before and after acid activation. The surface of brut clay is rough and uneven whereas, after acid activation, the clay surface is rough, raptured and porous. This change in the morphological properties is due to the removal of metals from the surface of the clay, making it more porous and rough.

The FTIR analysis was conducted with the raw clay, activated clay and MR activated clay in order to identify the functional groups involved in the adsorption (Fig. 4). The broad band at 3613 cm^{-1} is due to $^{-}$OH of interlayer water while the peak 1432 cm^{-1} is attributed to the stretching vibration of adsorbed water. The bands at 780 and 689 cm^{-1} referred to Si–O and Si–O–Si, respectively, attest the presence of tetrahedral silica layers. For the activated clay adsorbing MR (Fig. 4 d), we notice that the intensity of the peak at 990 cm^{-1} increased after the MR adsorption.

Effects of physical parameters on the MR adsorption

Contact time

The influence of the contact time on the MR removal onto the activated clay is carried out at MR dye

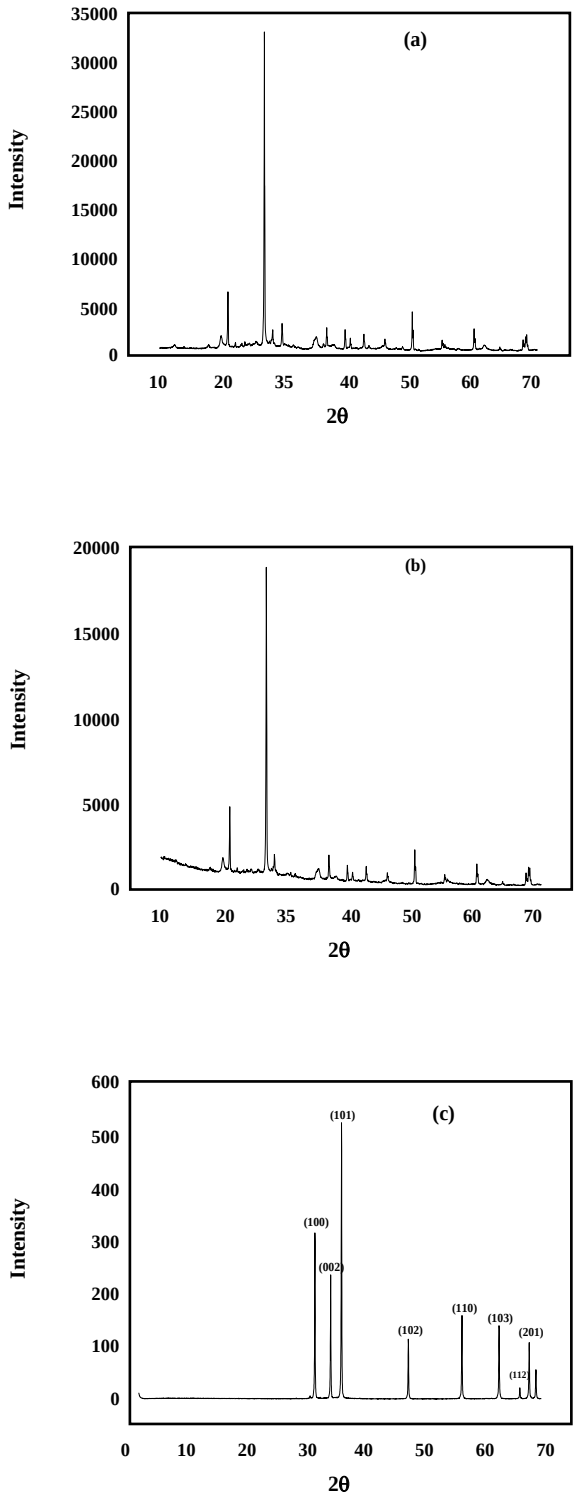

Fig. 2: XRD patterns of (a) raw clay (b) activated clay and (c) ZnO semiconductor.

concentration of 50 mg/L, adsorbent dose of 0.5 g/L, temperature of 298 K and pH ~ 7 (Fig. 5).Three different stages are clearly distinguished in the curve: the first one represents the instantaneous adsorption of MR which occurs within 15 min, the second stage shows a progressive equilibrium up to 60 min with a tendency to saturation while the third stage indicates the reached equilibrium, similar kinetic behavior was already reported elsewhere [41].

Initial pH

The pH is a controlling parameter that strongly affects the MR adsorption on the surface of activated clay. Its influence on the MR adsorption was studied over the pH range (3 - 9). The effect of initial solution pH on the Cr(VI) adsorption on activated clays was studied at the conditions of contact time, 120 min; adsorbent dosage, 0.5 g; and temperature, 25 °C. The results (Fig. 6) indicate a maximum MR removal (96 %) at neutral pH ~ 7, close to that of the environmental medium. The results show that the adsorption efficiency of MR increases with augmenting pH. At low pH, the number of H^+ ions increases, thus bridging the ligands between the adsorbent and MR molecules. As the pH increases, the number of OH^- ions increases and attract cationc ions MR for the adsorption on the clay. Similar results were reported for the MR adsorption on different adsorbents [42-44]; therefore, pH ~ 7 was selected for the further studies.

Adsorbent dose

The adsorbent dose is also important to take into consideration; it determines the uptake capacity of adsorbent for a given MR concentration. The effect of activated clay dose for the MR removal was studied in the range (0.1 - 1 g/L) for an initial MR concentration (C_i) of 50 mg/L and pH ~ 7 and at temperature of 298 K (Fig. 7). The dose was varied from 0.1 to 1 g/L; keeping constant the MR concentration. As expected the MR adsorption increases with raising the dose of activated clay and remains almost constant beyond 0.5 g/L. This may be simply due to the increased availability of surface active sites resulting from the increased dose and conglomeration of the adsorbent; the saturation is attributed to the occupation of active sites [44].

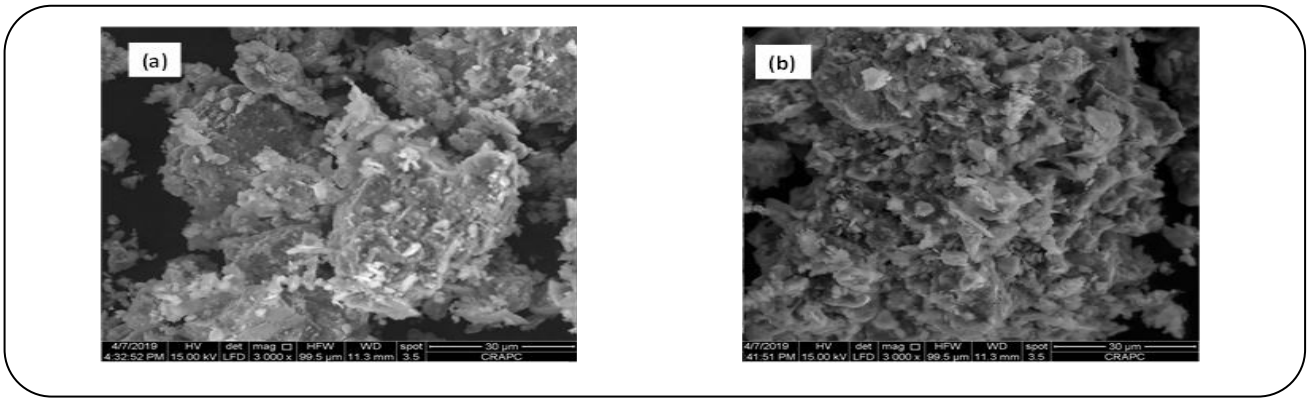

Fig. 3: SEM images of (a) raw clay (b) activated clay sample.

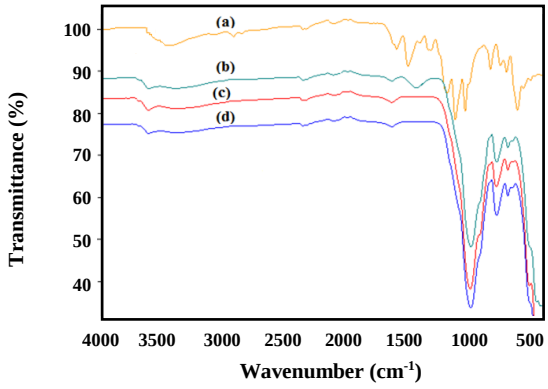

Fig. 4: FT-IR spectra of (a) MR dye, (b) raw clay, (c) activated clay, (d) activated clay after adsorption.

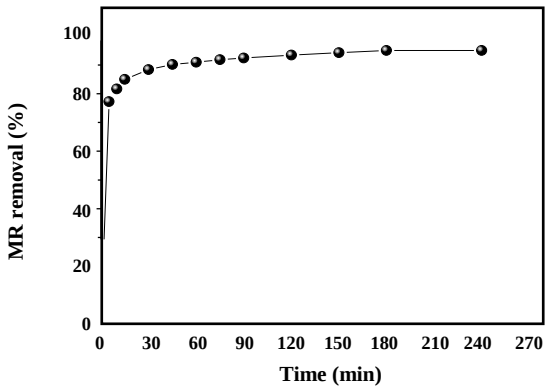

Fig. 5: Effect of contact time on the removal of MR on activated clay (C_{in} = 50 mg/L, pH ~ 7, adsorbent dose = 0.5 g/L and T = 25 °C).

Initial concentration

The effect of MR concentration was investigated in the range (25 - 125 mg/L) with the optimized clay dose of 0.5 g/L, pH ~ 7, a temperature of 25 °C and duration of 2 h. Fig. 8 shows the dependence of the adsorption rate on the initial MR concentration (C_{in}). The percentage of MR removal decreases from 97 to 66% from 25 to 125 mg/L. It is obvious that the MR removal is dependent on its concentration since the increased C_{in} improves the amount of the adsorbed dye. This retention at low MR concentrations is due to the available active sites on the adsorbent. However, the increase of MR concentration leads to a rapid saturation of active sites, resulting in decreased removal efficiency [44].

Temperature

The adsorption of MR on activated clay was carried at 25, 30, 40 and 50 °C, maintaining the pH, initial concentration C_{in} at their optimal values: however in order to study the effect of temperature we have taken a clay dose at 0.25 g/L instead of 0.5 g/L (Fig. 9). It can be observed that the adsorption percentage decreases 82 to 73% with raising the temperature from 25 to 50 °C. This is due to either the damage of active binding sites in the adsorbent or the increasing tendency to desorb the dye from the interface toward the solution. Such results indicate the exothermic nature of the adsorption process [45].

Modeling adsorption isotherm

The adsorption isotherms show the dependence of the adsorbed amount per unit mass of the clay versus the initial MR concentration (C_{in}). The maximum adsorption capacity is determined by using the adsorption isotherm models. The most commonly used isotherms for modeling adsorption processes in liquid phase are those of Freundlich, Langmuir, Temkin and Dubinin Radushkevich (D-R) models [46-49]. The isotherms help to design the suitable experimental system and to evaluate it and to find

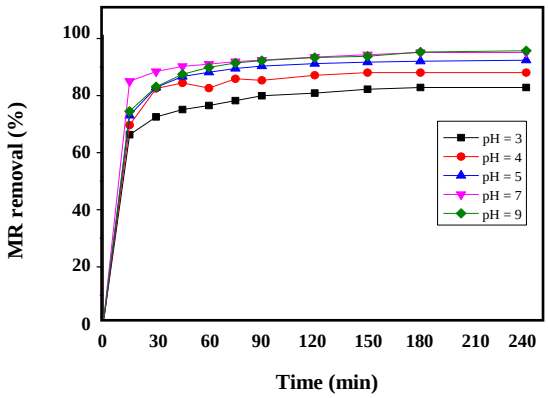

Fig. 6: Effect of solution pH on the MR removal on activated clay (C_{in} = 50 mg/L, adsorbent dose = 0.5 g/L and T = 25 °C).

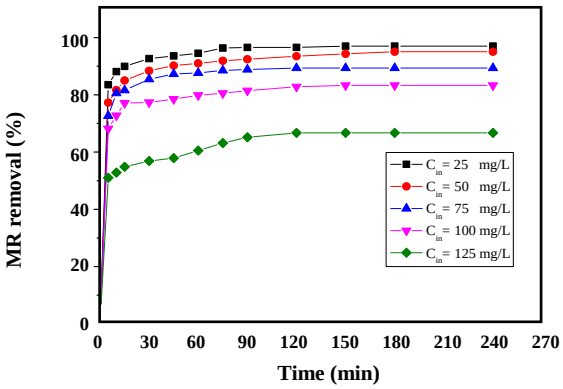

Fig. 8: Effect of initial concentration and contact time on the removal of MR onto activated clay (pH = 7, adsorbent dose = 0.5 g/L and T = 25 °C).

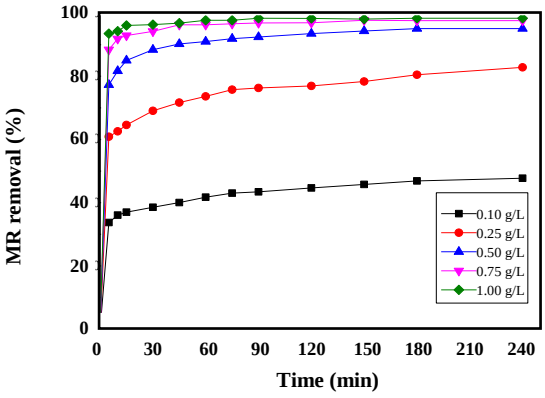

Fig. 7: Effect of adsorbent dose of activated clay on the removal of MR (pH = 7, C_{in} = 50 mg/L and T = 25 °C).

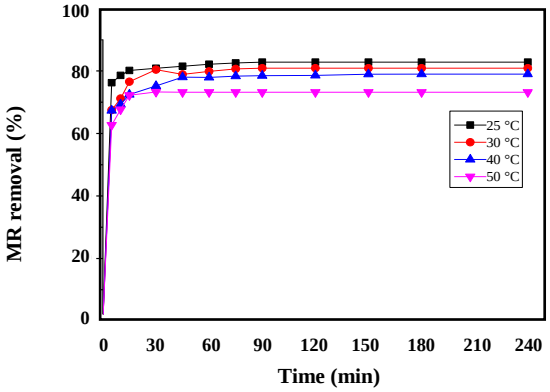

Fig. 9: Effect of temperature on the removal of MR on activated clay (pH = 7, C_{in} = 50 mg/L and adsorbent dose = 0.25 g/L).

out a deviation between experimental data and isotherm models. The adsorption isotherms are helping to describe surface processes of adsorbent, type of adsorbate monolayer or multilayer and maximum adsorption capacity of adsorbent, used for this work. Parameters of Freundlich, Langmuir, Temkin and Dubinin Radushkevich (D-R) isotherm models are calculated and presented in Table 1.

Where C_e is the equilibrium MR concentration(mg/L); q_e is the amount of MR adsorbed per gram of the adsorbent at equilibrium(mg/g); q_m is saturated monolayer adsorption capacity; b is Langmuir isotherm constant; K_F is the Freundlich constant [(mg/g)(L/mg) $^{1/n}$]; n is the heterogenity factor; K: constant related to the adsorption energy, q_{max} is the maximum amount of *MR* adsorbed per unit mass adsorbent (mg/g); β is the Dubinin–Radushkevich constant and ε is Polanyi potential (ε = RTln (1+ 1/C_e).

Dubinin-Radushkevich isotherm model does not assume a homogenous surface or constant adsorption potential. It is used to determine the nature of adsorption process and the mean energy of adsorption. The D-R isotherm equation and its linear form are represented in the Table 1. The mean free energy of adsorption (E_{ads}) can be calculated using the Equation (5):

$$E_{ads} = \frac{1}{\sqrt{2\beta}} \quad (5)$$

The best fit, suitability, and agreement isotherm models were validated using three statistical models:

Table 1: General forms of isotherm models used in this study.

Isotherm model	Functional form	Linear form	Plot
Langmuir	$q_e = \frac{q_m b C_e}{1 + bC_e}$	$\frac{C_e}{q_e} = \frac{1}{q_m b} + \frac{C_e}{q_m}$	C_e/q_e vs C_e
Freundlich	$q_e = K_F C_e^{\frac{1}{n}}$	$\ln q_e = \ln K_F + \frac{1}{n} \ln C_e$	$\ln q_e$ vs $\ln C_e$
Temkin	$q_e = \frac{RT}{b_T} \ln(K_T C_e)$	$q_e = \frac{RT}{b_T} \ln K_T + \frac{RT}{b_T} \ln C_e$	q_e vs $\ln C_e$
Dubinin Radushkevich	$q_e = q_{max} \exp(-\beta \varepsilon^2)$	$\ln q_e = \ln q_{max} - \beta \varepsilon^2$	$\ln q_e$ vs ε^2

sum of square error (SSE), chi-square test ($\chi 2$), and normalized standard deviation (Δq). The Sum of Square Error (SSE) is widely used and its mathematical expression is given [50]:

$$SSE = \sum_{i=1}^{n} (q_{e.exp} - q_{e.cal})^2 \quad (6)$$

Better agreement between the experimental quantity adsorbed and the calculated quantity adsorbed can be judged using this tool [51].

The chi-square test measures the difference between the experimental ($q_{e,exp}$) and calculated adsorbed amounts ($q_{e,exp}$ and ($q_{e,cal}$). The value of chi-square depends on the agreement between $q_{e,exp}$ and $q_{e,cal}$. If data evaluated from the model are similar to experimental data, χ^2 would be small and differ, χ^2 for large values [52].

$$\chi^2 = \sum_{i=1}^{n} \frac{(q_{e.exp} - q_{e.cal})^2}{q_{e.cal}} \quad (7)$$

The normalized standard deviation Δq (%) is evaluated using Equation (8). The isotherm model to describe the adsorption is validated by the normalized standard deviation, Δq (%) [50].

where n is the number of data points. Lower value of Δq (%) indicates good fit between experimental and calculated data.

$$\Delta q(\%) = 100 \times \sqrt{\frac{\sum_{i=1}^{n} \left(\frac{q_{e.exp} - q_{e.cal}}{q_{e.cal}} \right)^2}{n - 1}} \quad (8)$$

Based on R^2 and relatively low SEE, χ^2, and Δq presented in Table 2, the isotherm models fit the equilibrium data well in the following order: Langmuir > Temkin > Temkin > Dubinin–Raduskevich > Freundlich.

Therefore, it can be assumed that the adsorption occurs uniformly on the active sides of the adsorbent and is favorable when n lies between 1 and 10. In this case, n works out to be 3.21 (Table 2), indicating a favorable adsorption and the validity of the Freundlich model. The values of the Temkin isotherm parameters listed in Table 2 suggest a uniform distribution of the binding energy up to the maximum value.

The essential characteristics of the Langmuir isotherm is expressed in terms of dimensionless constant separation factor (R_L) [44; 48]:

$$R_L = \frac{1}{(1 + b\ C_{in})} \quad (9)$$

R_L characterizes the shape of the isotherm: unfavorable ($R_L > 1$), linear ($R_L = 1$), favorable ($0 < R < 1$), or irreversible ($R_L = 0$); R_L values between 0 and 1 give a favorable adsorption. In the present investigation, R_L lies between 0.071 and 0.188, showing a favorable adsorption.

The value of E_{ads} is useful for determine the type of adsorption. The E_{ads} value between 8 and 16 kJ/mol corresponds to chemical adsorption process while values smaller than 8 kJ/mol give a physisorption [49-54]. The experimental value (3.41 kJ/mol) indicates a physical adsorption process.

Adsorption kinetics study

The kinetic model of solute adsorption at the interfaces solid/solution is usually complex. The adsorption rate is highly dependent on several parameters such as the status of the solid matrix that has generally heterogeneous reactive sites, and physicochemical conditions of adsorption. Several kinetic models are available in the literature to describe the mechanism of adsorption. In this work, the adsorption of MR onto activated clay was investigated by the pseudo first-order, pseudo second-order and intraparticle diffusion and film diffusion models, with the aim of selecting the one able to provide the best kinetic description of the process.

Table 2: The Langmuir, Freundlich, Temkin and Dubinin–Radushkevich isotherms parameters for the adsorption of MR onto activated clay.

Model	Parameters	Value
Langmuir	q_m (mg/g)	175.65
	b (L/mg)	0.52
	R_L	0.071– 0.188
	R^2	0.9938
	SSE	151.133
	$\chi 2$	1.044
	Δq(%)	2.155
Freundlich	KF (mg/g)(L/mg) 1/n	62.69
	n	3.21
	R^2	0.8503
	SSE	1806.72
	$\chi 2$	15962.32
	Δq(%)	53.73
Temkin	K_T (L/mg)	7.88
	b_T (J/mol)	79.33
	R^2	0.9557
	SSE	475.24
	$\chi 2$	3.48
	Δq(%)	4.73
Dubinin–Radushkevich	q_{max} (mg/g)	198.48
	ε (mol^2/KJ^2)	4.30×10^8
	R^2	0.8615
	E_{ads} (kJ/mol)	3.41
	SSE	1696.51
	$\chi 2$	44.69
	Δq(%)	87.27

The Lagergren equation is the earliest known model describing the adsorption rate in the solute-adsorbent systems and is widely used for the pseudo first order kinetic [55-58]:

$$\frac{dq}{dt} = k_1 (q_e - q_t) \quad (10)$$

Where k_1 is the pseudo first order adsorption rate coefficient (min^{-1}). The integrated form of Eq. (10) for the boundary conditions (t = 0 to t and q_t = 0 to q_t) becomes:

$$\log (q_e - q_t) = \log q_e - \frac{k_1 t}{2.303} \quad (11)$$

The k_1 values are obtained from the slopes of linear plots $\log (q_e - q_t)$ versus the time t.

The second order kinetic is tested on the basis of the following equation [55-58]:

$$\frac{dq}{dt} = k_2 (q_e - q_t)^2 \quad (12)$$

k_2 is the pseudo second order adsorption rate coefficient (g/mg min). For the boundary condition, Eq. (9) becomes:

$$\frac{t}{q_t} = \frac{1}{\left(k_2 q_e^2\right)} + \frac{1}{q_e} t \quad (13)$$

In the adsorption system if intraparticle diffusion is the rate-controlling factor, percentage of the adsorbate varies with the square root of time as described by Weber and Morris [59-61]. The equation on the intraparticle diffusion model is given by following equation:

$$q_t = k_{in} t^{1/2} + C \quad (14)$$

where k_{in} is the internal diffusion coefficient (mg/g $min^{1/2}$), q_t the amount (mg/g) of MR adsorbed at time t (min) the sorption time; the constant C can be obtained from the slope and intercept of the plot q_t versus $t^{1/2}$.

The data were modeled using the pseudo first order model, pseudo second order model and intraparticle diffusion models for MR removal were tested with experimental data at different pHs, adsorbent dose and initial concentrations and at different temperatures. The rate constants, correlation coefficients (R^2), and the theoretical adsorption capacity were calculated for the three models according to Equations 11, 13 and 14 and are summarized in Table 3.

From the results obtained, the theoretical adsorption capacity calculated by pseudo first order kinetics is lower than the experimental value and the correlation coefficient was low. However, the plot of t/q versus t shows a good linearity indicating that the adsorption follows a pseudo second order mechanism. The pseudo second order kinetics was the model that gave the best fit to the experimental data (its correlation coefficients are higher than 0.9999, while those for pseudo first order are $0.6959 < R^2 < 0.9898$). Indeed, the correlation coefficient has been proposed as a good criterion for selection of a kinetic model. The theoretical adsorption capacity determined by the pseudo second order kinetics differs from the experimental values by only 3%, and the correlation coefficient R^2 is higher than 0.9999 for all studied parameters. A pseudo second order adsorption mechanism assumes that the rate of occupying adsorption sites is proportional to the square of the number of unoccupied sites [62].

The intraparticle diffusion model considers the adsorption of MR onto activated clay occurs in a three stage process : the rapid adsorption stage can be attributed to the diffusion of adsorbate through the solution to the external surface of the adsorbent or the boundary layer diffusion of the adsorbate molecules, the gradual adsorption stage, where intraparticle diffusion is rate controlled and the final equilibrium stage where intraparticle diffusion starts to slow down due to extremely low adsorbate concentrations in the solution [63-64]. The kinetic data were processed to determine whether intraparticle diffusion was the rate limiting step or not. From the results obtained (Fig. 13), the straight line did not pass through the origin, suggesting that the intraparticle diffusion was not only the rate controlling step [64]. The result showed that the adsorption process was complex and involved more than one mechanism. The straight lines obtained when fitting experimental data did not pass through the origin, also indicating that pore diffusion was not the only controlling step [56; 64]. The multilinearity of simulated curves for the test data indicates that two or more steps occurred in the adsorption process. The first straight portion is attributed to the fast mass transfer of adsorbate molecule from the bulk solution to the adsorbent surface and the second linear portion to the intra-particle diffusion.

Kinetic parameters for adsorption of MR dye onto activated clay are given in Table 3. Based on the correlation coefficients values, the R^2 of the pseudo second order model are higher than those for the intraparticle diffusion model, suggesting a chemical reaction mechanism [54].

Thermodynamic analysis

Temperature is important parameter in the adsorption studies because some important thermodynamic parameters such as enthalpy change (ΔH°), entropy change (ΔS°), and Gibbs free energy change (ΔG°) could be determined by using the following equations [65-70].

$$K_D = \frac{q_e}{C_e} \quad (15)$$

$$\Delta G^\circ = -RT \ln K_D \quad (16)$$

$$\Delta G^\circ = \Delta H^\circ - T\Delta S^\circ \quad (17)$$

$$\ln K_D = \frac{\Delta S^\circ}{R} - \frac{\Delta H^\circ}{RT} \quad (18)$$

Where K_D is the distribution factor (amounts of MR

Table 3: Parameters of pseudo-first-order, pseudo-second-order and intraparticle diffusion models for the MR adsorption onto acivated clay.

		pseudo first ordre			pseudo second ordre			intraparticle diffusion			
	$q_{e,\ exp}$	$q_{e,\ cal}$	$k_1 \cdot 10_2$	R^2	$q_{e,\ cal}$	$k_2 \cdot 10^3$	R^2	C	K_{in}	R^2	MR removal
	(mg/g)	(mg/g)	(min^{-1})		(mg/g)	(g/mg.min)		(mg/g)	(g/mg.min)		(%)
pH											
3	82.83	20.24	2.01	0.9836	85.03	2.14	0.9998	58.07	2.41	0.9364	82.83
4	88.03	16.37	2.37	0.8096	89.61	3.12	0.9998	62.02	2.92	0.6247	88.03
5	92.4	21.65	2.56	0.9643	94.07	2.7	0.9999	62.29	3.35	0.8731	92.4
7	95.7	11.43	1.67	0.9826	96.25	3.48	0.9999	80.13	1.41	0.9431	95.7
9	95.8	23.21	1.91	0.9512	97.66	1.97	0.9999	62.42	3.52	0.9378	95.8
S/L (g/L)											
0.1	238.6	67.69	1.29	0.9898	241.55	0.61	0.9982	157.17	6.56	0.9477	47.72
0.25	165.62	37.98	2.37	0.9811	158.23	1.84	0.9998	110.01	5.01	0.9942	82.81
0.5	95.7	14.55	1.96	0.9487	95.88	4.34	0.9999	72.47	2.81	0.9202	95.7
0.75	64.58	4.38	2.31	0.8699	65.32	17.66	0.9999	57.36	1.03	0.8871	96.88
1	124.19	2.61	3.07	0.8806	49.36	36.78	0.9999	46.13	0.36	0.7763	98.37
C_o (mg/L)											
25	48.51	6.2	3.16	0.9223	48.83	15.52	0.9999	40.77	0.91	0.8608	97.03
50	95.08	14.55	1.96	0.9487	95.88	4.34	0.9998	73.91	2.41	0.9003	95.08
75	134.04	21.71	3.83	0.9746	134.95	5.67	0.9999	106.05	3.65	0.8064	89.36
100	166.59	27.85	2.53	0.9279	168.07	2.69	0.9998	133.61	3.63	0.7419	83.3
125	166.75	48.45	2.39	0.9016	170.36	1.29	0.9992	119.63	4.01	0.9688	66.7
T(°C)											
25	165.62	28.07	5.52	0.7375	166.11	10.5	0.9999	147.71	2.76	0.7824	82.81
30	161.78	38.42	5.97	0.6959	162.6	6.74	0.9999	117.81	8.14	0.9263	80.84
40	157.94	39.13	4.74	0.8273	158.98	5.17	0.9999	123.83	4.97	0.9508	78.97
50	146.38	123.73	27.27	0.9532	146.63	19.54	0.9999	114.13	6.45	0.7449	73.19

Table 4: Thermodynamic parameters for the RM adsorption on activated clay.

T(K)	ΔH° (kJ/mol)	ΔS° (J/mol K)	ΔG° (kJ/mol)
298	-17.138	-32.84	-7.329
303			-7.12
313			-7.05
323			-6.419

Table 5: Comparison of the maximum adsorption capacity q_m of some adsorbents.

Adsorbents	Adsorption capacity (mg/g)	Reference
Silica	3.03	[72]
Bentonite	33.78	[73]
Natural sugarcane stalks powder	20.96	[74]
Acivated Algerian clay	175.74	Present work
Treated Algerian natural phosphates	29.06	[75]
Activated carbons from surplus sewage sludge	188	[76]

adsorbed per gram of activated clay divided by its concentration in the liquid phase), R (8.314 J/mol/K) is the universal gas constant and T is the temperature in Kelvin

It can therefore be ascertained from Table 4 that the adsorption process is exothermic because the value of ΔH° is negative (-17.138 kJ/mol), the standard entropy change ΔS° (-32.84 J/mol K) show that the adsorption is done with increasing order at the solid-solution interface during the MR adsorption. This entropy is used to describe the randomness at the solid-solution interface during the adsorption process. The negative free enthalpy ΔG° indicates a spontaneous adsorption and its decrease with increasing temperature confirms the feasibility of the MR adsorption. The negative values of the standard Gibbs free energy (ΔG°) indicate the viability, feasibility, and spontaneity of the adsorption process. According to the literature, the change in free energy for physisorption is usually between −20 and 0 kJ/mol, whereas that for chemisorption is often in the range of −80 to – 400 kJ/ mol [44; 71]. The Δ*G*° value obtained in this research indicated that the adsorption is physisorption.

Comparison of q_{max} adsorbents with other adsorbents of MR dye

The comparison of the adsorption capacities of the activated clay with materials used in the open literature reveals better results. Table 5 compares the maximum adsorption capacities q_m (mg/g) on various adsorbents and shows that our activated clay adsorbs better than the zeolites, biomass materials and others clays all have substantially lower adsorption capacity. Therefore, it appears that the abundance of this material and its ability to remove the dye with high performances are beneficial and promising for the environmental protection.

Photodegradation of MR by ZnO

Effect of operating parameters on the photodegradation of MR dye

The adsorption reduces considerably the MR concentration but not enough to comply with the directives of the water standards. At low concentrations, the photocatalysis takes over to eliminate by advanced oxidation process (AOPs) the remaining MR concentration (C_r) on illuminated ZnO suspension acting as an infinity of micro-photoelectrochemical cells. In order to determine the photocatalytic performance of ZnO, it is imperative to study the variation of the main physico-chemical parameters namely the contact time; ZnO dose and MR concentration (C_r).

Contact time

The photocatalytic degradation of MR was carried out after a dark adsorption on ZnO which occurs in ~ 60 min at pH ~ 7, ZnO dose of 1 g/L and a concentration C_r of 16.7 mg/L.

It is worthwhile to mention that ZnO is stable in the pH range (4-12); above and before if dissolves respectively into ZnO_2^{2-} and Zn^{2+}. The kinetic (Fig. 10) shows that MR disappears almost completely (95%) after 2 h of exposition to solar irradiation (~ 970 mW/cm^2).

Catalyst dose

In order to determine the optimal dose of ZnO for a maximum absorption of incident photons, we have varied the dose in the range (0.1 - 1 g/L) at 25 °C keeping the MR concentration at 16.7 mg/L and pH ~ 7.

We can see that the degradation yield increases with raising the ZnO dose to reach an optimum of 0.5 g/L followed by a plateau region when further ZnO was added (Fig. 11). Such enhancement is simply due to the higher reception surface for the incident photons, generating a high number of $HO^{\bullet}$ and $O_2^{\bullet-}$ radicals, respectively in the valence and conduction bands which participate in the MR degradation through AOP mechanism. The plateau region is due to the shadowing effect and light scattering which limit the reception surface area. The scattering light and shadow effect also account for this saturation.

Remaining MR concentration C_r

To determine the effect of the remaining MR concentration on the course of the reaction, we have varied C_r in the domain (2.5 – 41.3 mg/L) by maintaining the ZnO dose and pH at their optimal values, 0.5 g/L and 7 respectively and ambient temperature (Fig. 16).

Mechanism of photodegradation

The MR degradation takes place within a short period at low concentrations due to the decreased number of MR molecules by adsorption. *Boughelout et al.* [76] explained this phenomenon by the fact that when the number of molecules of the substrate is low, the competition for the photogenerated reactive species ($HO^{\bullet}$, h^+, e^- ..) is small and the availability of the latter becomes relatively larger. By contrast, the increased concentration weakens the light flux, in accordance with the Beer Lambert law, and in this way the number of photons reaching the catalyst surface.

The iso-electric point of ZnO is found to be 7.5 and the attachment of MR by electrostatic interactions on the catalyst should facilitate the electron transfer. Fig. 10 gives the UV-Visible spectra of MR solution under solar light. The decrease of the absorbance at 530 nm over

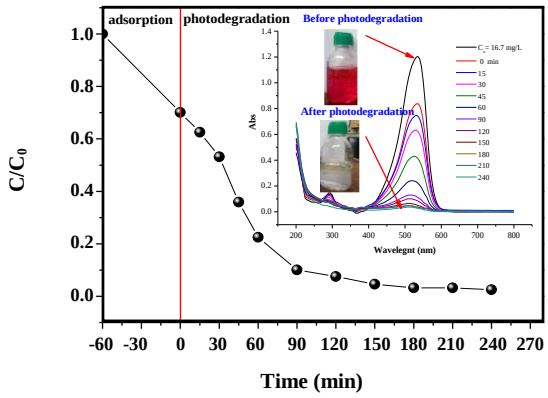

Fig. 10: Effect of contact time on the photodegradation of MR on ZnO (C_o ~ 16.7 mg/L, pH = 7, adsorbent dose = 1 g/L).

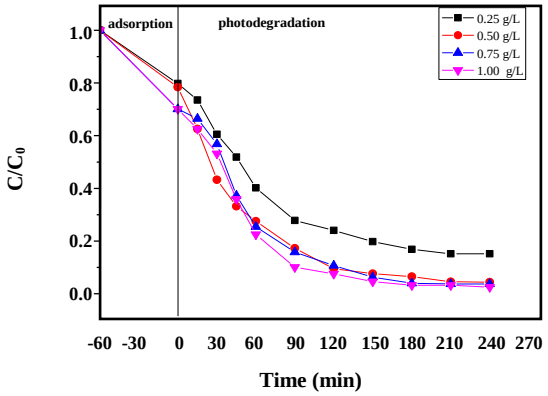

Fig. 11: Effect of the catalyst dose on the photodegradation of MR onto ZnO (pH ~ 7 and C_o = 16.7 mg/L).

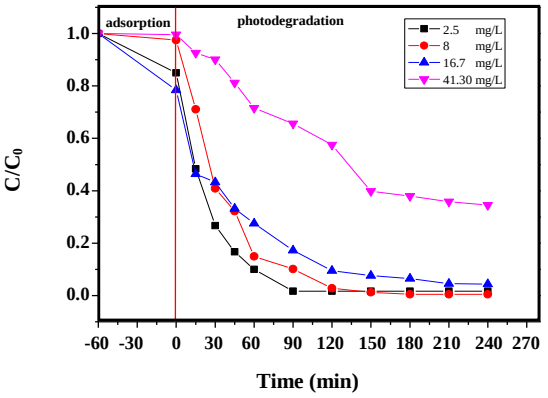

Fig. 12: Effect of initial concentration on the photodegradation of MR onto ZnO (pH = 7 and catalyst dose = 0.5 g/L).

irradiation time is due to MR light induced oxidation since MR is not degraded by photolysis. The photo-electrochemical reactions occurring at the interface are the following [76]:

$$ZnO + h\nu \xrightarrow{UV} h^{+}_{VB} + e^{-}_{CB} \quad (19)$$

$$e^{-}_{CB} + O_2 \rightarrow O_2^{\bullet} \quad (20)$$

$$h^{+}_{VB} + H_2O \rightarrow OH^{\bullet} + H^{+} \quad (21)$$

$$H_2O^{\bullet} + H^{+} \rightarrow H_2O_2 \quad (22)$$

$$OH^{\bullet} + O_2^{\bullet} + dye \rightarrow CO_2 + H_2O \quad (23)$$

The potential of $O_2/O_2^{\bullet}$ couple (~ -0.5 V) is less cathodic than ZnO-CB (~ -0.83 V_{SCE}) [77-78], and the photoelectrons generate $O_2^{\bullet}$ radicals responsible of the MR degradation. Concomitantly, the holes in the valence band (2.37 V) permit the oxidation of water by $OH^{\bullet}$ radical, resulting in prolonged lifetime of carriers.

Photodegradation kinetics

To describe the kinetics of the MR degradation, we were inspired by the results reported in the literature [34]. In most cases, the kinetics of the photodegradation of organic molecules are described by a first-order model:

$$r = -\frac{dC}{dt} = k_{app}.C \quad (24)$$

Where *r* is the rate and k_{app} (mn^{-1}) the apparent first-order rate constant; the integration of Eq. (21) gives:

$$\ln\frac{C_o}{C} = k_{app}.t \quad (25)$$

The plots ln (C_o/C) as a function of time for each studied parameter are linear, indicating a first order. The constant k_{app} is characteristic of photocatalytic process in agreement with the Langmuir-Hinshelwood (L-H) model and the hypothesis evokes the case of a diluted medium [34]. Fig. 13 show that the rate of MR disappearance can be described by a first order kinetic.

The k_{app} values make it possible to deduce two other parameters of major interest, namely the initial rate (v_o) for which the dye MR degrades with a half-time ($t_{1/2}$) given by [79]:

$$t_{1/2} = \frac{\ln 2}{k_{app}} \quad (23)$$

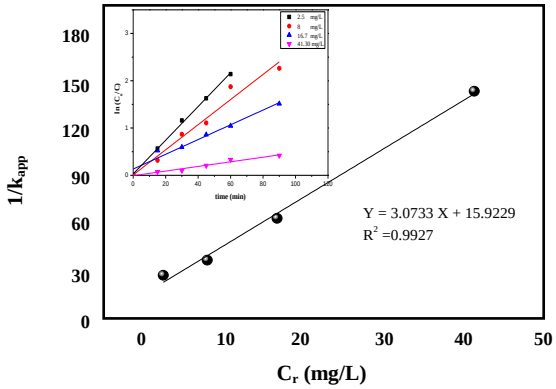

Fig. 13: Application of Langmuir –Hinshlwood model.

The corresponding half times and rate constants k_{app} were calculated by plotting the ln(C_o/C) versus time, whose derived values are presented in Table 6.

Table 6 shows that the initial degradation rate increases with the initial MR concentration (C_r), which improves the overall photocatalytic efficiency by promoting contact MR substrate with the photogenerated species degradation rate falls above C_r value of 2.5 mg/L because the MR molecules can absorb a significant amount of incident light, thus reducing the production of hole/electron (e^-/h^+) pairs.

As shown in Table 4, MR dye degradation follows the pseudo-first order kinetic model. The rate constant increase with the ZnO concentration and approaches a limit value at 1 g/L of catalyst. However, The apparent rate constant k_{app} decreased with the increasing in the initial concentration of MR when other parameters are maintained unchanged.

Modeling of degradation kinetics by the Langmuir-Hinshelwood

The photocatalysis involves an electronic transfer described by the L-H model, about the oxidation kinetic of organic pollutants. This formalism relies on the fact that the organic molecules before their photodegradation, are adsorbed according to the Langmuir model. The degradation rate at different MR concentrations, indicates that although the MR adsorption is low on the catalyst surface (~ 8%), it plays an important role in photocatalysis owing to the physical contact; the relation linking the rate to the concentration of the substrate:

$$v = k_{app}.C = \frac{k_r k_s C}{1 + k_s C} \quad (26)$$

Table 6: Value of kinetic constants, times of half reaction for different catalyst dose and MR concentration.

	$k_{app} \times 10^2$ (min^{-1})	R^2	$t_{1/2}$ (min)	MR photodegradation (%)
Catalyst dose (g/L)				
0.25	1.091	0.9766	63.53	81.05
0.5	1.602	0.9875	43.27	94.43
0.75	1.702	0.9846	40.72	94.72
1	1.97	0.9745	35.18	96.4
C_r (mg/L)				
2.5	3.563	0.9975	19.45	99.48
8	2.657	0.9625	26.08	98.03
16.7	1.602	0.9875	43.27	94.43
41.3	0.48	0.9624	144.41	65.32

Where k_r (mg/L min) and k_s (L/mg) are the reaction rate and adsorption constants respectively.

$$\frac{1}{k_{app}} = \frac{1}{k_r k_s} + \frac{C_r}{k_r} \quad (27)$$

The graphical representation of $1/k_{app}$ as a function of C_r, is linear and confirms the validity of the L-H model (R^2 = 0.9927) (Fig. 13). The slope and the intercept of the straight line $1/k_{app}$ against C_r give the constants k_r (32.53 × 10^{-2} mg/L min) and k_s (19.30 × 10^{-2} L/mg).

CONCLUSIONS

The purpose of this study was devoted to the utilization of abundant clay to adsorb the Maxilon Red, a dye threatening the aquatic environment. The work consists of the preparation of activated clay by acid attack for the treatment of the dye, used in the textile industry. The physical parameters revealed that the MR adsorption on activated clay increases with pH and indicated a gradual removal of the dye with temperature. Raising the adsorbent dose increased the adsorption removal and peaks at of 0.5 g/L. The maximum adsorption capacity of the activated clay of 175 mg/g is higher than most capacities mentioned in the literature in which the authors used expensive materials. The kinetic studies showed that the MR removal is rapid and obeys to the pseudo second order model with a strong affinity for the activated clay surface The material presents an exothermal behavior and the free energy indicated a spontaneous adsorption.

The combined adsorption/photocatalysis has significantly improves the MR elimination up to 100%. In summary, we can say that our objective was reached but must be broadened for applications to other types of pollution, and especially the mineral pollution.

Acknowledgments

This work was financially supported by the Mechanic and Engineering Process Faculty and Chemistry (USTHB, Algiers).

Received : Jun. 29, 2019 ; Accepted : Oct. 21, 2019

REFERENCES

[1] Khemila B., Merzouk B., Chouder A., Zidelkhir R., Leclerc J. P., Lapicque F., Removal of a Textile Dye Using Photovoltaic Electrocoagulation, *Sustain. Chem. Pharm.*, **7:** 27–35 (2018).

[2] Abidi N., Duplay J., Jada A., Errais E., Ghazi M., Semhi K., Trabelsi-Ayadi M., Removal of Anionic Dye from Textile Industries' Effluents by Using Tunisian Clays as Adsorbents. Zeta Potential and Streaming-Induced Potential Measurements, *C. R. Chimie.*, **22**: 113–125 (2018).

[3] Ventura-Camargo B.C., Marin-Morales M.A., Azo Dyes: Characterization and Toxicity A Review, *Text. Light Ind. Sci. Technol.*, **2**: 85–103 (2013).

[4] Chaari I., Fakhfakh E., Medhioub M., Jamoussi F., Comparative Study on Adsorption of Cationic and Anionic Dyes by Smectite Rich Natural Clays, *J. Mol. Struct*, **1179**: 672–677 (2019).

[5] Mittal H., Alhassan S. M., Ray, S. S., Efficient Organic Dye Removal from Wastewater by Magnetic Carbonaceous Adsorbent Prepared from Corn Starch, *J. Environ. Chem. Eng.*, **6(6)**: 7119–7131 (2018).

[6] El Haddad M., Removal of Basic Fuchsin Dye from Water Using Mussel Shell Biomass Waste as an Adsorbent: Equilibrium, Kinetics, and Thermodynamics, *J. Taibah Univ. Sci.* **10**: 664–674 (2016).

[7] Dogan M., Karaoglu M. H., Mahir Alkana., Adsorption Kinetics of Maxilon Yellow 4GL and Maxilon Red GRL Dyes on Kaolinite, *J. Hazard. Mater*, **165**:1142–1151 (2009).

[8] Mehrabi, F., Vafaei, A., Ghaedi, M., Ghaedi, A. M., Dil, E. A., Asfaram, A., Ultrasound Assisted Extraction Of Maxilon Red GRL Dye from Water Samples Using Cobalt Ferrite Nanoparticles Loaded on Activated Carbon as Sorbent: Optimization and Modeling, *Ultrason. Sonochem*., **38**:672–680 (2017).

[9] Doğan, M., Karaoğlu, M. H., Alkan, M., Adsorption Kinetics of Maxilon Yellow 4GL and Maxilon Red GRL Dyes on Kaolinite, *J. Hazard. Mater*., **165(1-3)**: 1142–1151 (2009).

[10] Basibuyuk M., Forster C. F., An Examination of the Adsorption Characteristics of a Basic Dye (Maxilon Red BL-N) on to Live Activated Sludge System, *Process Biochem.*, **38(9)**: 1311–1316 (2003).

[11] Katheresan V., Kansedo J., Lau S. Y., Efficiency of Various Recent Wastewater Dye Removal Methods: A Review, *J. Environ. Chem. Eng.*, **6**: 4676-4697 (2018).

[12] Sharma A., Syed Z., Brighu U., Gupta A. B., Ram, C., Adsorption of Textile Wastewater on Alkali-Activated Sand, *J. Clean. Prod.*, **220**: 23–32 (2019).

[13] Liang J., Ning X. A., Sun J., Song J., Hong Y., Cai, H., An integrated Permanganate and Ozone Process for the Treatment of Textile Dyeing Wastewater: Efficiency and Mechanism, *J. Clean. Prod.*, **204**: 12–19 (2018).

[14] Özcan A., Öncü E. M., Özcan A. S., Kinetics, Isotherm and Thermodynamic Studies of Adsorption of Acid Blue 193 from Aqueous Solutions onto Natural Sepiolite, *Colloid. Surface A.*, **277(1-3)**: 90–97 (2006).

[15] Karaoglu M. H., Dogan M., Alkan M., Removal of Cationic Dyes by Kaolinite, *Micropor. Mesopor. Mat*., **122**: 20–27(2009).

[16] Tahir H., Muhammad A., Alam A., Bibi Jamil R., Qadri M., Structural Modifications of Surfactant-Assisted Alumina and Their Effectiveness for the Removal of Dyes, *Iran. J. Chem. Chem. Eng. (IJCCE)*, **37(1)**:47–60 (2018).

[17] Hernández-Montoya V., Pérez-Cruz M. A., Mendoza-Castillo D. I., Moreno-Virgen M. R., Bonilla-Petriciolet A., Competitive Adsorption of Dyes and Heavy Metals on Zeolitic Structures, *J. Environ. Manag.*, **116:** 213–221 (2013).

[18] Li Y., Du Q., Liu T., Peng X., Wang J., Sun J., Xia L., Comparative Study of Methylene Blue Dye Adsorption onto Activated Carbon, Graphene Oxide, And Carbon Nanotubes, *Chem. Eng. Res. Des*, **91(2)**: 361–368 (2013).

[19] Dehghani M. H., Naghizadeh A., Rashidi A., Derakhshani E., Adsorption of Reactive Blue 29 Dye from Aqueous Solution by Multiwall Carbon Nanotubes, *Desalin. Water Treat.*, **51(40-42)**: 7655–7662 (2013).

[20] Naghizadeh A., Ghafouri, M., Synthesis and Performance Evaluation of Chitosan Prepared from Persian Gulf Shrimp Shell in Removal of Reactive Blue 29 Dye from Aqueous Solution (Isotherm, Thermodynamic and Kinetic Study), *Iran. J. Chem. Chem. Eng. (IJCCE)*, **36(3)**: 25–36 (2017).

[21] Kamranifar M., Naghizadeh A. Montmorillonite Nanoparticles in Removal of Textile Dyes from Aqueous Solutions: Study of Kinetics and Thermodynamics, *Iran. J. Chem. Chem. Eng. (IJCCE)*, **36(6)**:127–137 (2017).

[22] Kausar A., Iqbal M., Javed A., Aftab K., Bhatti H. N., Nouren S., Dyes Adsorption Using Clay and Modified Day: A Review, *J. Mol. Liq.*, **256**: 395–407 (2018).

[23] Yener J., Kopac T., Dogu G., Dogu T., Adsorption of Basic Yellow 28 from Aqueous Solutions with Clinoptilolite and Amberlite, *J. Colloid. Interf. Sci*., **294**: 255–264 (2006).

[24] España V. A. A., Sarkar B., Biswas B., Rusmin R., Naidu, R., Environmental Applications of Thermally Modified and Acid Activated Clay Minerals: Current Status of the Art, *Environ. Technol. Innov.*, **13**: 383-397 (2016).

[25] Kausar A., Iqbal M., Javed A., Aftab K., Bhatti H. N., Nouren S., Dyes Adsorption Using Clay and Modified Clay: A Review, *Journal of Molecular Liquids*, **256**: 395–407 (2018).

[26] Martínez-López S., Lucas-Abellán C., Serrano-Martínez A., Mercader-Ros M. T., Cuartero N., Navarro P., Pérez S., Gabaldon J. A., Gómez-López V. M., Pulsed Light for a Cleaner Dyeing Industry: Azo Dye Degradation by an Advanced Oxidation Process Driven by Pulsed Light, *J. Clean. Prod.*, **217**:757–766 (2019).

[27] Zaharia C., Suteu, D. Muresan A., Muresan R., Popescu A., Textile Wastewater Treatment by Homogenous Oxidation with Hydrogen Peroxide, *Environ. Eng. Manag. J.*, **8(6)**: 1359–1369 (2009).

[28] Zou X. L., Combination of Ozonation, Activated Carbon, and Biological Aerated Filter for Advanced Treatment of Dyeing Wastewater for Reuse, *Environ. Sci. Pollut Res.*, **22(11)**: 8174–8181 (2015).

[29] Soon A. N., Hameed B. H., Heterogeneous Catalytic Treatment of Synthetic Dyes in Aqueous Media Using Fenton and Photo-Assisted Fenton Process, *Desalination*, **269(1-3)**:1–16 (2011).

[30] Shaida M. A., Sen A. K., Dutta R. K., Alternate Use of Sulphur Rich Coals as Solar Photo-Fenton Agent for Degradation of Toxic Azo Dyes, *J. Clean. Prod.*, **195**: 1003–1014 (2018).

[31] Bendjama H., Merouani S., Hamdaoui O., Bouhelassa M., UV-Photolysis of Chlorazol Black in Aqueous Media: Process Intensification Using Acetone and Evidence of Methyl Radical Implication in the Degradation Process, *J. Photoch. Photobio A.*, **368**: 268–275 (2019).

[32] Chakma S., Moholkar V. S., Mechanistic Analysis of Sono-Photolysis Degradation of Carmoisine, *J. Ind. Eng. Chem.*, **33**: 276–287 (2016).

[33] Alireza N. E., Setareh Khorsandi S., Photocatalytic Degradation of 4-Nitrophenol with ZnO Supported Nano-Clinoptilolite Zeolite, *J. Ind. Eng. Chem.*, **20(3)**: 937–946 (2014).

[34] Mekatel H., Amokrane S., Bellal B., Trari M., Nibou D., Photocatalytic Reduction of Cr(VI) on Nanosized Fe2O3 Supported on Natural Algerian Clay: Characteristics, Kinetic and Thermodynamic Study, *Chem. Eng. J.*, **200**:611–618 (2012).

[35] Vinayagam M., Ramachandran S., Ramya V., Sivasamy A., Photocatalytic Degradation of Orange G Dye Using ZnO/Biomass Activated Carbon Nanocomposite, *J. Environ. Chem. Eng.*, **6**: 3726–3734(2018).

[36] Zhu H., Jiang R., Fu Y., Guan Y., Yao J., Xiao L., Effective Photocatalytic Decolorization of Methyl Orange Utilizing TiO_2/ZnO/Chitosan Nanocomposite Films under Simulated Solar Irradiation, *Desalination*, **286**: 41–8 (2012).

[37] Nasrallah N., Kebir M., Koudri Z., Trari M., Photocatalytic Reduction of Cr(VI) on the Novel Hetero-System $CuFe_2O_4$/CdS, *J. Hazard. Mater.*, **185(2-3)**: 1398–1404 (2011).

[38] Zhang Y., Tang Z. R., Fu X., Xu Y.J., TiO_2-Graphene Nanocomposites for Gas-Phase Photocatalytic Degradation of Volatile Aromatic Pollutant: TiO2-Graphene Truly Different from other TiO_2-Carbon Composite Materials, *ACS Nano.*, **4**: 7303–7314 (2010).

[39] Kamranifar, M., Naghizadeh, A., Montmorillonite Nanoparticles in Removal of Textile Dyes from Aqueous Solutions: Study of Kinetics and Thermodynamics, *Iran. J. Chem. Chem. Eng. (IJCCE)*, **36(6)**: 127–137 (2017).

[40] Bergaya F. Theng B. K. G., Lagaly G., General Introduction: Clays, Clay Minerals, and Clay Science, *Handbook of Clay Science: Developments in Clay Science*, **1**: 1–18 (2006).

[41] Ratnamala G.M., Deshannavar U.B., Munyal S., Tashildar K., Patil S., Shinde A., Adsorption of Reactive Blue Dye from Aqueous Solutions Using Sawdust as Adsorbent: Optimization, Kinetic, and Equilibrium Studies, *Arab. J. Sci. Eng.*, **41(2)**: 333–344 (2016).

[42] Olgun A., Atar N., Equilibrium and Kinetic Adsorption Study of Basic Yellow 28 and Basic Red 46 by a Boron Industry Waste, *J. Hazard. Mater.*, **161(1)**: 148–156 (2009).

[43] Yagub M.T., Sen T.K., Afroze S., Ang H.M., Dye and Its Removal from Aqueous Solution by Adsorption: A Review, *Adv. Colloid. Interface.*, **209**: 172-184(2014).

[44] Subramani S.E., Thinakaran N., Isotherm, Kinetic and Thermodynamic Studies on the Adsorption Behaviour of Textile Dyes onto Chitosan, *Process. Saf. Environ.*, **106**:1–10 (2017).

[45] Aid A., Amokrane S., Nibou D., Mekatel E., Trari M., Hulea V., Modeling Biosorption of Cr (VI) onto Ulva Compressa L. from Aqueous Solutions, *Wat. Sci. Tech.*, **77 (1)**: 60–69 (2018).

[46] Naghizadeh A., Nabizadeh R., Removal of Reactive Blue 29 Dye by Adsorption on Modified Chitosan in the Presence of Hydrogen Peroxide, *Environ. Protect. Eng.*, **42(1)**: - (2016).

[47] Abdelnaeim, M. Y., El Sherif, I. Y., Attia, A. A., Fathy, N. A., & El-Shahat, M. F.. Impact of chemical Activation on the Adsorption Performance of Common Reed Towards Cu (II) and Cd (II). *Int. J. Miner. Process.*, **157**: 80–88 (2016).

[48] Göçenoğlu Sarıkaya A., Osman B., Kara, A., Evaluation of the Effectiveness of Microparticle-Embedded Cryogel System in Removal of 17 B-Estradiol from Aqueous Solution, *Desalin. Water Treat.*, **57(33)**: 15570-15579 (2016).

[49] Osman B., Özer E. T., Kara A., Yeşilova E., Beşirli N., Properties of Magnetic Microbeads in Removing Bisphenol-A from Aqueous Phase, *J. Porous Mat.*, **22(1)**: 37–46 (2015).

[50] Dada A. O., Adekola F. A., Odebunmi E. O., Kinetics, Mechanism, Isotherm and Thermodynamic Studies of Liquid Phase Adsorption of Pb^{2+} onto Wood Activated Carbon Supported Zerovalent Iron (WAC-ZVI) nanocomposite, *Cogent Chemistry*, **3(1)**: 1351653 (2017).

[51] Boparai H. K., Joseph M., O'Carroll D. M., Kinetics and thermodynamics of Cadmium ion Removal by Adsorption onto Nano Zerovalent Iron Particles, *J. Hazard. Mater.*, **186(1)**: 458-465 (2011).

[52] Ahmad, M. A., Puad, N. A. A., Bello, O. S. Kinetic, Equilibrium and Thermodynamic Studies of Synthetic Dye Removal Using Pomegranate Peel Activated Carbon Prepared by Microwave-Induced KOH Activation, *Water Resour. Ind.*, **6:**18-35 (2014).

[53] Kara A., Demirbel E., Tekin N., Osman B., Beşirli, N., Magnetic Vinylphenyl Boronic Acid Microparticles for Cr(VI) Adsorption: Kinetic, Isotherm and Thermodynamic Studies, *J. Hazard. Mater.*, **286**: 612–623 (2015).

[54] Nibou D., Mekatel H., Amokrane S., Barkat M., Trari M., Adsorption of Zn^{2+} Ions onto Naa And Nax Zeolites: Kinetic, Equilibrium and Thermodynamic Studies, *J. Hazard. Mater.*, **173**: 637–646 (2010).

[55] Ho Y., McKay G., A comparison of Chemisorption Kinetic Models Applied to Pollutant Removal on Various Sorbents, *Process. Saf. Environ. Prot.*, **76 (4)**: 332–340 (1998).

[56] Wei C., Song X., Wang Q., Hu Z., Sorption Kinetics, Isotherms and Mechanisms of PFOS on Soils with Different Physicochemical Properties, *Ecotox. Environ. Safe.*, **142**: 40–50 (2017).

[57] Safieh K. A. A., Al-Degs Y.S., Sunjuk M.S., Selective Removal of Dibenzothiophene From Commercial Diesel Using Manganese Dioxide-Modified Activated Carbon: A Kinetic Study, *Environ. Technol.*, **36(1)**: 98–105 (2015).

[58] Yeşilova E., Osman B., Kara A., Özer E. T., Molecularly Imprinted Particle Embedded Composite Cryogel for Selective Tetracycline Adsorption, *Sep. Purif. Technol.*, **200**: 155–163 (2018).

[59] Wu F. C., Tseng R. L., Juang, R. S., Initial Behavior of Intraparticle Diffusion Model Used in the Description of Adsorption Kinetics, *Chem. Eng. J.*, **153(1-3)**: 1–8 (2009).

[60] Weber W.J., Morris J.C., Kinetics of Adsorption on Carbon Solution, *J. San. Eng. Div. ASCE.*, **89**: 31–59 (1963).

[61] Syafiuddin A., Salmiati S., Jonbi J., Fulazzaky M. A., Application of the Kinetic and Isotherm Models for Better Understanding of the Behaviors of Silver Nanoparticles Adsorption onto Different Adsorbents, *J. Environ. Manag.*, **218**: 59–70 (2018).

[62] Gupta V. K., Agarwal S., Saleh T. A., Synthesis And Characterization of Aluminacoated Carbon Nanotubes and their Application for Lead Removal, *J. Hazard. Mater.***185 (1)**: 17–23 (2011).

[63] Magdy Y. H., Altaher H., Kinetic Analysis of the Adsorption of Dyes from High Strength Wastewater on Cement Kiln Dust, *J. Environ. Chem. Eng.*, **6**: 834–841 (2018).

[64] Yao C., Chen T., A Film-Diffusion-Based Adsorption Kinetic Equation and Its Application, *Chem. Eng. Res. Des.*, **119**: 87–92 (2017).

[65] Li Z., Liu G., Su Q., Jin X., Wen X., Zhang G., Huang R., Kinetics and Thermodynamics of NPX Adsorption by Γ-Feooh in Aqueous Media, *Arab. J. Chem.*, **11(6)**: 910–917 (2018).

[66] Abbas M., Kaddour S., Trari M., Kinetic and Equilibrium Studies of Cobalt Adsorption on Apricot Stone Activated Carbon, *J. Ind. Eng. Chem.*, **20(3)**: 745–751 (2014).

[67] Naghizadeh, A., Ghafouri, M. Synthesis and Performance Evaluation of Chitosan Prepared from Persian Gulf Shrimp Shell in Removal of Reactive Blue 29 Dye from Aqueous Solution (Isotherm, Thermodynamic and Kinetic Study), *Iran. J. Chem. Chem. Eng. (IJCCE)*, **36(3)**: 25–36 (2017).

[68] Hadadi N., Kananpanah S., Abolghasemi H., Equilibrium and Thermodynamic Studies of Cesium Adsorption on Natural Vermiculite and Optimization of Operation Conditions, *Iran. J. Chem. Chem. Eng. (IJCCE)*, **28(4)**: 29–36 (2009).

[69] Derakhshani E., Naghizadeh A., Optimization of Humic Acid Removal by Adsorption Onto Bentonite and Montmorillonite Nanoparticles, *J. Mol. Liq.*, **259**: 76–81 (2018).

[70] Naghizadeh A., Ghafouri M., Jafari A., Investigation of Equilibrium, Kinetics and Thermodynamics of Extracted Chitin from Shrimp Shell In Reactive Blue 29 (RB-29) Removal From Aqueous Solutions, *Desalin. Water Treat.*, **70**: 355–363 (2017).

[71] Kara A., Tekin N., Alan A., Şafaklı A., Physicochemical parameters of Hg (II) Ions Adsorption from Aqueous Solution by Sepiolite/poly (vinylimidazole), *J. Environ. Chem. Eng.*, **4(2)**: 1642–1652 (2016).

[72] Koyuncu M., Removal of Maxilon Red GRL from Aqueous Solutions by Adsorption onto Silica, *Orient. J. Chem.*, **25(1)**: 35–40 (2009).

[73] Koyuncu M., Adsorption Properties of Basic Dyes (Maxilon Red GRL and Maxilon Yellow GRL) onto Bentonite, *Asian. J. Chem.*, **21(7)**: 5458–5464 (2009).

[74] El-Sayed G. O., Mohammed T. Y., Salama, A. A. A, Batch Adsorption of Maxilon red GRL from Aqueous Solution by Natural Sugarcane Stalks Powder, *ISRN. Environ. Chem.*, **2**: 1–8 (2013).

[74] Graba Z., Hamoudi S., Bekka D., Bezzi N., Boukherroub R., Influence of Adsorption Parameters of Basic Red Dye 46 by the Rough and Treated Algerian Natural Phosphates, *J. Ind. Eng. Chem.*, **25**: 229–238 (2015).

[75] Martin M. J., Artola A., Balaguer M. D., Rigola, M., Activated Carbons Developed from Surplus Sewage Sludge for the Removal of Dyes from Dilute Aqueous Solutions, *Chem. Eng. J.*, **94(3)**: 231–239 (2003).

[76] Boughelout A., Zebbar N., Macaluso R., Zohour Z., Bensouilah A., Zaffora A., Trari, M., Rhodamine (B) Photocatalysis under Solar Light on High Crystalline ZnO Films Grown by Home-Made DC Sputtering Optik, *International Journal for Light and Electron Optics.*, **174** :77–85 (2018).

[77] Chabane L., Zebbar N., Kechouane M., Aida M. S., Trari M., Al-Doped and in-Doped ZnO Thin Films in Heterojunctions with Silicon, *Thin Solid Films*, **605**: 57–63 (2016).

[78] Ameen S., Akhtar M. S., Shin H. S., Speedy Photocatalytic Degradation of Bromophenol Dye over ZnO Nanoflowers, *Mate. Lett.*, **209** :150–154 (2017).

[79] Chekir N., Tassalit D., Benhabiles O., Merzouk N. K., Ghenna M., Abdessemed A., Issaadi R., A Comparative Study of Tartrazine Degradation Using UV and Solar Fixed Bed Reactors, *Int. J. Hydrogen Energ.*, **42(13)**: 8948–8954 (2017).